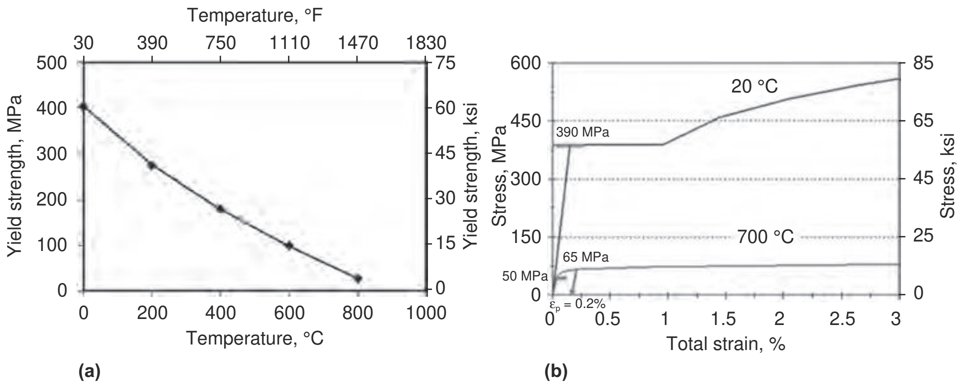

Fig. 11 (a) Yield limit of spheroidized and annealed SAE 52100 as a function of temperature. (b) Corresponding stress-strain curves; strain rate: 40 × 10−4 1/s. Source: Ref 4

stress—and arises only if stress and phase transformation exist simultaneously (Ref 8). If this condition is fulfilled, transformation plasticity will occur. This mechanism works for all types of transformations (Ref 9):

- Formation of austenite from a ferritic phase
- Formation of martensite from austenite
- Formation of bainite from austenite
- Formation of pearlite from austenite

The proportionality constant between the amount of transformation plasticity and stress deviator depends on the type of transformation (Ref 9).

Figure 12 shows the length changes of samples from steel grade SAE 4140H during martensitic hardening for different loads. A stress that is given to the sample before the transformation starts will modify the stress-free curve considerably. The aforementioned proportionality constant has a value of 4.2×10^{-5} N/mm^2 (Ref 10) for the given conditions. This means that a stress of 50 N/mm^2 leads to a plastic deformation of 0.2% at the end of the transformation.

In a component with a banded microstructure, transformation plasticity occurs on a mesoscopic scale and generates an anisotropic and position-dependent transformation strain. During heating of components with a banded ferritic-pearlitic microstructure, size and shape changes, especially on the macroscopic scale, can result. Details are given in the article “Distortion Engineering” in this Volume as well as in Ref 11.

Plastic Deformations by Creep. The third distortion-relevant mechanism also does not need a minimum stress value. Creep acts especially at elevated temperatures—higher than 33 to 50% of the melting temperature in Kelvin—and is a time-dependent effect (Fig. 13, Ref 4). Even at a moderate stress value of 5 MPa (0.7 ksi), a plastic deformation of 0.2% at a typical carburizing temperature of 940 °C (1725 °F) already results after 1 h.

The relevance of plasticity mechanisms for heat treatment is as follows:

- Transformation plasticity is an important distortion-relevant factor during each heating and cooling process if stresses are present.
- Yielding is most important during quenching. During heating, it can be relevant if the component contains huge residual stresses from the previous manufacturing steps (e.g., cold forming, machining).
- Creep is not relevant during quenching, because the temperature region of interest will be passed quite quickly. However, during heating, austenitizing, and carburizing, this mechanism can play an important role and must be kept in mind for the determination of possible sources of size and shape changes.

Systematization of Unavoidable Size and Shape Changes and Corresponding Stress Evolution

For the deduction of the systematization of unavoidable dimensional and shape changes and the corresponding stresses, a hypothetical experiment is presented in this section. This experiment is not realistic, but it helps to understand the generation of unavoidable distortion.

Size Changes by Transformation

In the hypothetical experiment, it is assumed that a component can be produced under ideal conditions, that is:

- A component with absolutely homogeneous chemical composition and homogeneous initial microstructure
- Without any texture
- A blank component without any residual stress can be produced by machining.

Furthermore, it must be presumed that heat treatment could be carried out under ideal conditions, including:

- Homogeneous heating of the component
- Very small heating rate

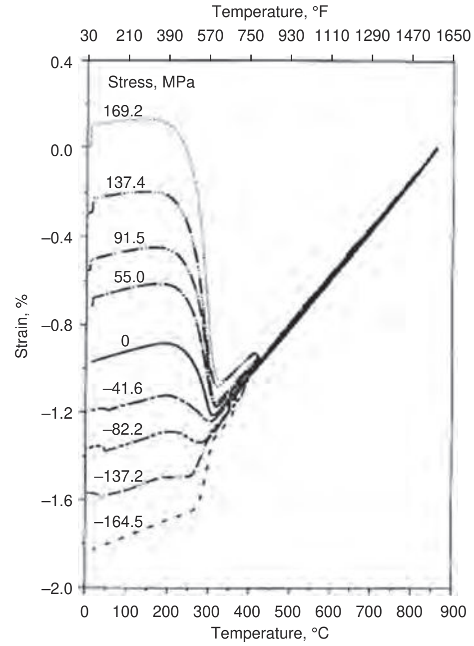

Fig. 12 Influence of stresses on length changes during martensitic hardening of 42CrMo4 (SAE 4140H). Source: Ref 10

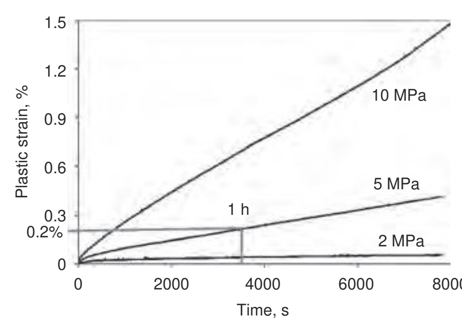

Fig. 13 Plastic deformation by creep at 940 °C (1725 ° F) for 20MnCr5 (SAE 5120). Source: Ref 4

- Ideal charging
- Minimum possible cooling rate
- Ideal heat-transfer conditions

Even under these perfect conditions, dimensional alterations will still occur if the heat treatment includes a change in the microstructure. Even without any plastic deformation, size changes unavoidably occur as a result of the relationship between specific volume and microstructure status (Fig. 8). This diagram shows, for example, that a martensitically hardened component made from steel with 0.4% C experiences an unavoidable reduction in volume as a result of normalizing with very slow cooling, because a ferritic/pearlitic microstructure is produced under these conditions. This example may not be practically relevant, but it indicates clearly the principle of unavoidable size changes as a result of phase transformation. In the systematization developed by Wyss for unavoidable changes in dimensions and shape, this case is referred to as tendency I (Fig. 14, Ref 12). In this figure, the dashed lines mark the original contour, and the continuous lines illustrate possible size changes after a heat treatment following the assumptions of the hypothetical experiment. Tendency I is characterized by pure dimensional changes without any shape change. The size changes depend on the following parameters:

- Chemical composition (especially carbon)
- Initial microstructure
- Austenitizing conditions
- Type of transformation
- Degree of transformation (partial, complete)

According to the assumptions of the hypothetical experiment, no stresses or residual stresses occur.

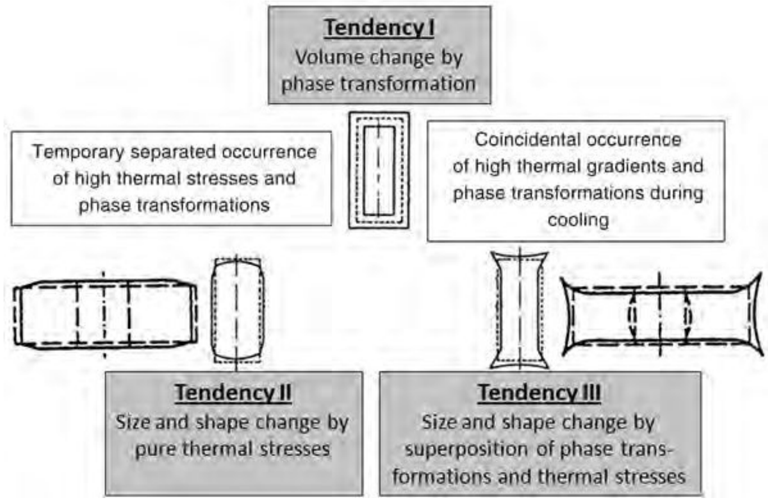

Fig. 14 Three basic tendencies of unavoidable changes in dimensions and shape. Source: Ref 12

Size and Shape Changes by Thermal Stresses

In the second step of the hypothetical experiment, the postulation of a minimum cooling rate is dropped to approach the real situation during a quenching process. The consequences are temperature differences within the component. For the moment, however, a transformation-free process is analyzed.

Stress Development and Residual-Stress State. As a result of the temperature dependency of the specific volume, the temperature differences create thermal stresses in the component. As indicated by the schematic cooling diagram in Fig. 15 (Ref 13), the near-surface layer of the material initially cools faster than the core. Therefore, the surface region tries to contract. This action is blocked by the hot core. Consequently, tensile stresses result in the near-surface layer (curve *a*) in equilibrium with compressive stresses in the core. When the highest temperature difference between surface and core has been reached (point *W*), the largest tensile stress value of the near-surface layer results. With time, the core contracts more rapidly than the near-surface layer, and the temperature difference and stresses decrease continuously. At the end of the cooling process, all stresses have disappeared.

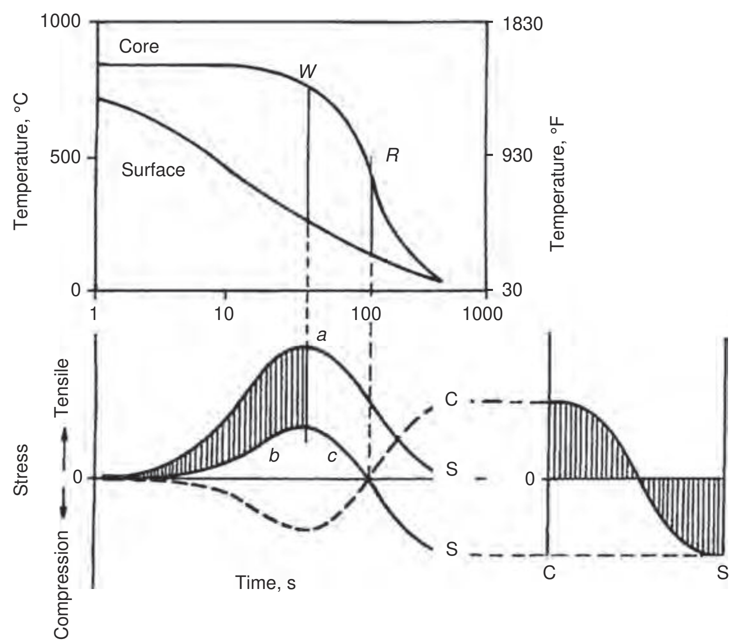

Fig. 15 Creation of thermal stresses. C, core; S, surface. Source: Ref 13

This purely elastic example works only if the equivalent stress does not reach the temperature-dependent yield limit during the complete quenching process. However, if the equivalent stress exceeds the yield strength of the steel, the exceeding stresses are eliminated by plastic deformation (shaded area of the lower diagram in Fig. 15), and the resulting stress follows curve *b*. After passing the maximum temperature difference, the stronger contraction of the core leads to an elastic reduction of the stresses at the surface (curve *c*) until the stress conditions in the material are reversed. Then, the surface of the material is exposed to compressive stresses and the core to tensile stresses. After temperatures in the material have fully equalized, the stress conditions schematically indicated in the bottom right of Fig. 15 remain in the material as residual stresses. This residual-stress distribution, with tensile stresses in the core and compressive stresses near the surface, is typical for quenched materials without phase transformation.

Size and Shape Changes. This analysis indicates that dimensional changes in this example are ultimately caused by local stresses in excess of the yield strength of the material and resulting plastic deformations. The corresponding changes in dimensions and shape can be described by the rule of Ameen. According to this rule, all materials experience changes in dimensions and shape, tending to approximate the shape of a sphere if only thermal stresses are present during quenching (Ref 14). Figure 16 (Ref 4) shows an originally square billet dead weight body of 100CrMn6 steel (0.90 to 1.05 wt% C, 0.40 to 0.70 wt% Si, 0.95 to 1.25 wt% Mn, and 0.35 to 1.60 wt% Cr) that was heated and quenched a few hundred times, which proves Ameen's rule very impressively.

In the systematization established by Wyss, this case is described as tendency II (Fig. 14): The larger dimension decreases and the other one increases. The effects of process and material parameters in this case can be described as follows (Ref 15). Size changes as a result of pure thermal stresses increase with:

- Increasing dimensions
- Increasing quenching temperature

- Increasing quenching rate
- Decreasing thermal conductivity
- Increasing thermal expansion
- Decreasing yield strength

Similar rules also apply to the heating process.

Influence of Biot Number on Size Changes. The rule of Ameen was found from the evaluation of quenching experiments with oil and water. But what happens for smaller cooling intensities? This question was pursued by Frerichs, who performed a large number of experimental and numerical investigations on the influence of dimensions and heat-transfer coefficient on size changes (Ref 16). He particularly investigated size changes after gas quenching. One important finding was that a dimensionless number named after the French physicist and mathematician Jean-Baptiste Biot can be used to describe the size changes of long cylinders. The term *long* in this context means that the length-to-diameter ratio must be at least 3.

The Biot number (*Bi*) is calculated by the ratio of heat transfer and heat conduction. Three parameters are included that characterize:

- The process by the heat-transfer coefficient, α
- The material by the heat conductivity, λ
- The component by a characteristic length, L

For the characteristic length, Frerichs at first chose the diameter (D) of the cylinders. He used the following definition:

$$Bi = \frac{\alpha}{\lambda} \cdot D \qquad \text{(Eq 12)}$$

The important second finding was that the dimensional changes of long cylinders without phase transformation after a quenching process depend only on the value of the Biot number and not on the value of the three defining parameters (Ref 16). Figure 17 shows a large number of simulations with different combinations of these three parameters. It can be seen that there are small "scatterings," but all curves are very similar and describe something similar to a master curve that depends only on the Biot number, as stated previously. This curve consists of three sections:

- $Bi < \approx 0.4$: No size changes; yield limit of the material will not be exceeded; no residual stresses after quenching
- $\approx 0.4 < Bi < \approx 3.2$: Positive length changes; negative diameter changes; typical residual-stress distribution
- $Bi > \approx 3.2$: Negative length changes; positive diameter changes mean the rule of Ameen is valid; typical residual-stress distribution

Therefore, the third finding of Frerichs is that the rule of Ameen is correct only if the quenching process under consideration results in a Biot number larger than approximately 3.2. This means that preferably quenching processes in oil and water will follow the rule of Ameen.

Influence of Plastic Strain on Size and Shape Changes. The reason for the existence of the change of sign of dimensional changes has not been given until now. To answer this question, Frerichs evaluated heat treatment simulations in more detail. Figure 18 (Ref 4) shows the distributions of axial plastic strain and residual axial stress for different Biot numbers. Up to the maximum length change in Fig. 17 (Biot number of approximately 1.3), positive values of plastic strain in axial directions predominate in the distribution of this property. For larger Biot numbers, the portion

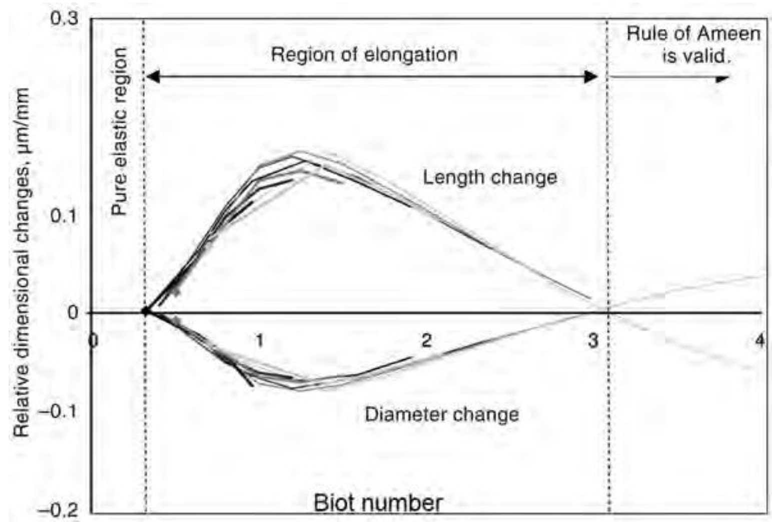

Fig. 17 Dimensional changes of long cylinders made of austenitic steel X8CrNiS18-9 (AISI 303) as a function of the Biot number. Source: Ref 16

Fig. 16 Originally square billet dead weight body after several hundred salt bath quenching processes. Source: Ref 4

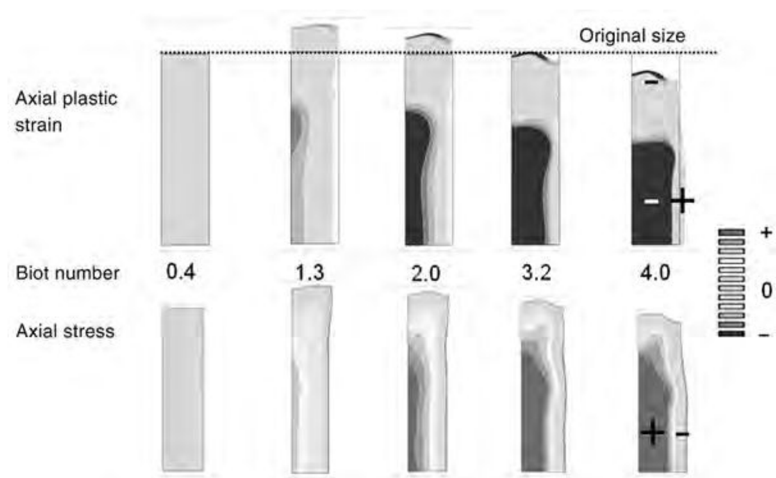

Fig. 18 Changes of contour and corresponding distributions of plastic deformations and residual stresses in axial direction for different values of Biot number. (Only a quarter of the cylinder cross section is shown.) Source: Ref 4

of the cross section with negative plastic strains in the axial direction continuously increase and lead to the observed length reduction for Biot numbers larger than 3.2.

Figure 18 shows another important result: For small Biot numbers, the contour of the cylindrical samples changes according to tendency III. Therefore, the systematization of Wyss (Fig. 14) also must be completed, and a differentiation in dependence on the Biot number must be added.

The Influence of Biot Number on Residual Stresses. Looking to the residual stresses as a function of the Biot number, the same trend can be found for the stress component in the axial direction: The portion of the cross section with tensile residual stresses in this direction increases (Fig. 18). However, in all cases, the typical stress distribution of quenching without phase transformation has resulted: tensile stresses in the core and compressive stresses near the surface. However, it must be mentioned that the simple two-shell model used in Fig. 15 is not valid near the face surface. Here, the complexity of the tensor characteristic of stresses must be taken into account.

The Influence of Geometry on Size Changes. To compare the size changes of different geometries, another more-general characteristic length must be used. Frerichs (Ref 17) followed a proposal by Kobasko (Ref 18) and used the ratio of volume (V) and surface (S) of the samples as the characteristic length. The Biot number then is given by:

$$Bi = \frac{\alpha}{\lambda} \cdot \frac{V}{S} \qquad \text{(Eq 13)}$$

The volume-to-surface ratio of long cylinders with diameter D can be calculated quite easily:

$$\frac{V}{S}(\text{Long cylinder}) \approx \frac{1}{4} \cdot D \qquad \text{(Eq 14)}$$

Consequently, this definition leads to smaller Biot numbers, and the correlation between the Biot numbers with the two different characteristic lengths is given by:

$$Bi\left(\frac{V}{S}\right) \approx \frac{1}{4} \cdot Bi(D) \text{ for long cylinders} \qquad \text{(Eq 15)}$$

Figure 19 compares simulation results of size changes for long cylinders, plates, and rings (Ref 17). The Biot numbers of first plastic deformations, extreme size changes, and change of sign are nearly the same for all investigated geometries. Furthermore, it can be concluded that the largest dimensions of the simple geometries (cylinder height, average ring radius, and plate radius) have a similar behaviour, as do the smallest dimensions (cylinder radius, ring wall thickness, and plate height). For the third dimension in between the extreme ones, no general conclusion is possible on the basis of the data in Fig. 19.

The Influence of Further Material and Process Parameters on Size Changes. It must be taken into account that the quantitative results given in Fig. 17 to 19 are valid only for the investigated melt of steel grade AISI 303. However, similar dependencies can be expected qualitatively for each material without phase transformation. Frerichs has shown that in addition to the Biot number, only five other dimensionless numbers are necessary for the description of thermal-stress-induced size changes of cylindrical bodies (Ref 17). The relative length and diameter changes are functions of:

$$\frac{\Delta L}{L} = f\left(\frac{\alpha}{\lambda} \cdot \frac{V}{S};\ \alpha_{th} \cdot (T_0 - T_q);\ \nu;\ \frac{E}{\sigma_0};\ \frac{E}{K};\ n\right)$$

$$\frac{\Delta D}{D} = g\left(\frac{\alpha}{\lambda} \cdot \frac{V}{S};\ \alpha_{th} \cdot (T_0 - T_q);\ \nu;\ \frac{E}{\sigma_0};\ \frac{E}{K};\ n\right) \qquad \text{(Eq 16)}$$

where α_{th} is the coefficient of thermal expansion; T_0 and T_q are the initial temperature and the temperature of the quenching medium, respectively; ν and E are elastic properties (Poisson's ratio and Young's modulus, respectively); and σ_0, K, and n are plastic properties (yield stress and parameters of a modified Ramberg-Osgood model, respectively) (Ref 17).

These dimensionless numbers were identified by use of the so-called analysis of dimensions, and the use of them offers two main advantages (Ref 19):

- If all relevant parameters describing geometry, material, and process are known, the dimensionless numbers governing the distortion behavior of this system can be deduced. Generally, the quantity of dimensionless numbers is smaller than the total amount of influencing parameters.
- If the values of all of the dimensionless numbers of two geometrically similar bodies are equal, then the distortion behavior of these two bodies also is equal.

The second statement is true even when all of the parameters defining the two configurations are totally different. In fluid dynamics, this nature of dimensionless numbers is the basis for the transferability of results, for example, obtained with a small model in a wind tunnel and transferable to a real car or an aircraft.

However, the analysis of dimensions cannot predict the functions g and f in Eq 16. A first approach was developed by Landek et al. (Ref 20). They used averaged material properties of 28 representative austenitic steels (Table 1) and the corresponding standard deviations. Based on these data, many finite-element simulations for long cylinders were completed. The resulting length changes were fitted by a nonlinear regression model. Figure 20 shows the comparison between the simulated and

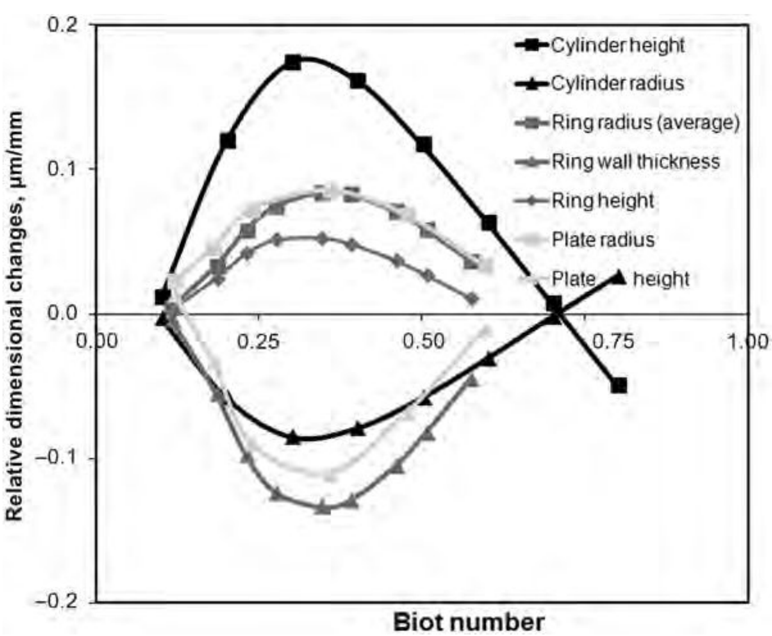

Fig. 19 Size changes of simple components without undergoing a phase transformation. Source: Ref 17

Table 1 Representative group of analyzed austenitic steels

Steel grades	Steel grades (continued)
27Cr-9Ni (as-cast)	AISI 301
19Cr-10Ni-2.5Mo	AISI 302
19Cr-9Ni-0.2C	AISI 304
19Cr-10Ni	AISI 305
19Cr-11Ni-2.5Mo	AISI 308
19Cr-9Ni	AISI 309
19Cr-11Ni-3.5Mo	AISI 310
24Cr-13Ni	AISI 314
25Cr-20Ni	AISI 315
X8CrNiS18.9	AISI 316
AISI 201	AISI 317
AISI 202	AISI 321
AISI 205	AISI 329
AISI 216	AISI 330

Source: Ref 20

calculated length changes. The correspondence is not perfect, but the regression model offers the possibility for an acceptable estimation of the length change when the parameters of Eq 16 are known.

Size Changes during a Heat Treatment Process. Up until now, all statements were made for distortion behavior as a result of a heat treatment process when the component has cooled down to room temperature at the end of the process. However, the concept of dimensionless numbers also works during a process. In this case, instead of time, the Fourier number (Fo) must be used:

$$\mathrm{Fo} = \frac{\lambda}{\rho \cdot c_p} \cdot \frac{t}{L^2} \quad \text{(Eq 17)}$$

where ρ is density, c_p is the specific heat capacity, t is time, and L is the characteristic length. Şimşir has shown that in addition to the cooling curves, all other time-dependent results of a quenching process (e.g., phase portions, components of stress and strain tensor) are equal if the values of all dimensionless numbers, including the Fourier number, of two geometrically similar bodies are equal (Ref 21).

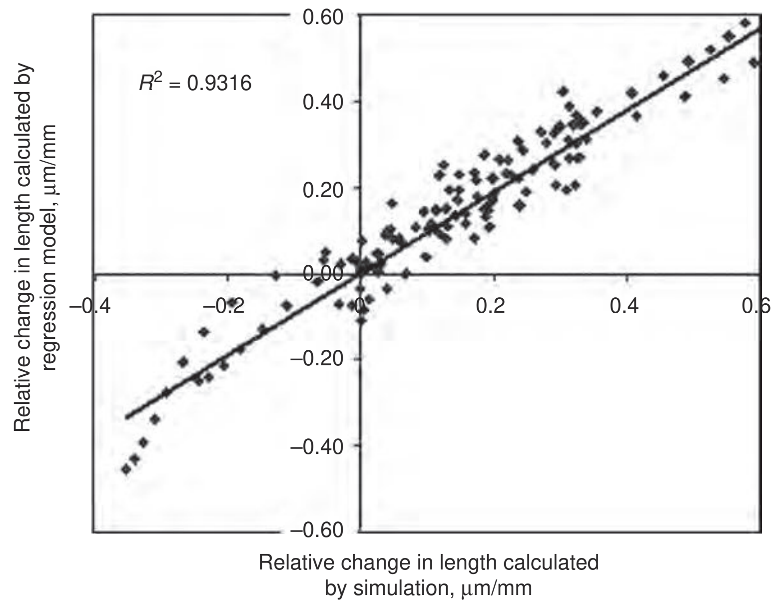

Fig. 20 Correspondence between length changes calculated by numerical simulations and predicted by a regression model after transformation-free cooling of bars made of austenitic steels. Source: Ref 20

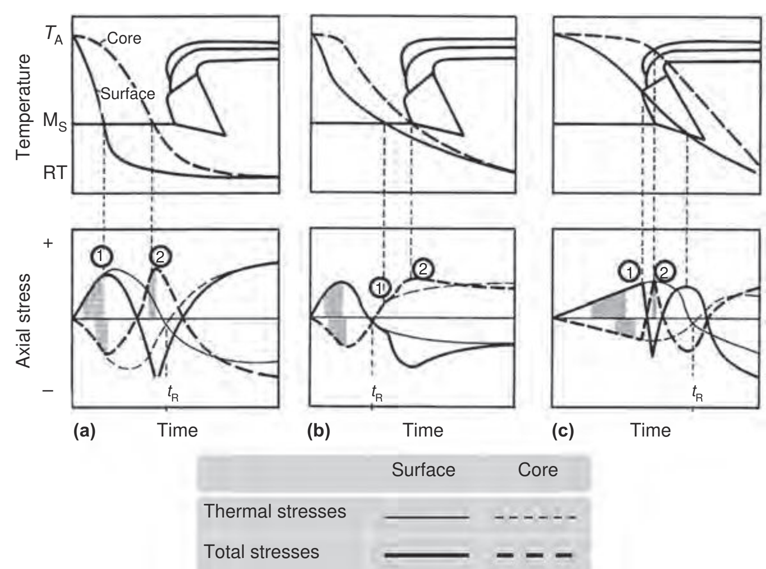

Fig. 21 Schematic examples for superpositions of thermal and transformation stress. Source: Ref 22

Size and Shape Changes by Superposition of Thermal Stresses and Transformations

In the last step of this systematization, it must be kept in mind that a hardening process needs phase transformations during quenching, and to achieve a specific microstructure, requirements for local cooling rates must be fulfilled. Consequently, the general example consists of a component with temperature gradients—and the corresponding thermal stresses—and phase transformations, depending on the local cooling curve. In contrast to the situation of distortion according to tendency I, phase transformation gradients exist here and will lead to transformation stresses. The superposition of both types of stresses results in a complex time-dependent stress profile in the component. The plastic deformations resulting from this profile during the quenching process via transformation plasticity and yielding form the final size and shape changes.

Stress Development and Residual-Stress State. Figure 21 shows three examples of different interactions between thermal and transformation stresses (Ref 22). The upper parts of the images show schematically a continuous cooling transformation diagram and cooling curves of the surface and core. The lower parts exhibit the corresponding stress development. For better understanding, the pure thermal and the total stresses are presented. Shaded regions in these diagrams indicate plastic deformations.

Martensitic Transformation before Change of Sign of Stresses. The example in Fig. 21(a) analyzes a fully martensitic transformation. Until the transformation of the near-surface region starts, only thermal stresses (thin lines) are generated, which are equivalent to Fig. 15. The martensite formation starts at the surface (point 1), and the local volume increases because of the larger specific volume of martensite (Fig. 8). As a consequence, compressive transformation stresses occur, and the total stress (thick line) is reduced. As a reaction, the stress in the core (dashed line) starts to increase, and plastic deformations resulting from yielding (shaded area) are stopped. The increase of the total core stresses continues until the transformation of the core starts (point 2). The same happens here as just described for the near-surface region. At the end of the quenching process, the residual-stress state consists of tensile stresses at the surface and compressive stresses in the core—opposite from the situation after quenching without transformation.

Martensitic Transformation after Change of Sign of Stresses. The example in Fig. 21(b) also deals with a fully martensitic hardening process. However, in this case, the transformation starts after the thermal stresses have changed their sign (time t_R). In this situation, the transformation stress at the surface amplifies the thermal stresses there. The total stress therefore becomes more negative. The reaction of the core increases the tensile stresses there. When the core starts to transform, the complete stress state is reduced only slightly. At the end of the quenching process, a residual-stress distribution results that is similar to the case of pure thermal stresses (Fig. 15).

Surface Transformation Starts before and Ends after Core Transformation. In Fig. 21(c), transformation of the near-surface region starts with bainite formation and ends with martensitic transformation. Between the beginning and end of these processes, the core transforms into ferrite and pearlite. This scenario contains three changes of the algebraic sign. At the end of the hardening process, residual-stress distribution of the thermal stress type again results.

These examples show that stress generation and the resulting residual-stress distribution depend a great deal on the interaction of cooling and transformation behavior, and, in general, prediction of the resulting residual-stress state is not possible without heat treatment simulation.

Size and Shape Changes. As shown previously, stress development depends in a complex way on the interactions between transformation and cooling behavior. The resulting size and shape changes in a simple cylinder or ring may vary between tendency I (only size changes), tendency II (spherical shape, size and shape changes), and tendency III (wire-reel, dimension and shape changes; see Fig. 14). If high thermal stresses and transformations occur at different times, the results will be between sheer size changes and the spherical shape. The size changes caused by transformations and the size and shape changes caused by thermal stresses are practically added to each other. On the other hand, if thermal stresses and transformation occur at the same time, the result is the wire reel (tendency III; Ref 12, 23).

In Fig. 22 (Ref 23), four cases of different interactions between thermal stresses and phase transformation and the resulting size and shape changes are shown.

Maximum Temperature Difference after Finishing of Transformation. In Fig. 22(a), a cylinder with a diameter of 100 mm (4 in.) and made from SAE 1015 steel grade was quenched in oil. The maximum temperature difference between surface and core (point *W*) occurs after the transformation was finished. Therefore, the resulting distortion corresponds to an approach to the spherical shape (tendency II).

Maximum Temperature Difference before Start of Transformation. If the steel grade is changed to X40Cr13 (0.4 to 0.5% C, <1% Si, <1% Mn, and 12 to 14% Cr) (Fig. 22b), then point *W* is reached before the transformation starts, and the distortion is similar to the example in Fig. 22(a).

Maximum Temperature Difference and Concurrent Core Transformation. In Fig. 22(c), a smaller cylinder with a diameter of 30 mm (1.2 in.) and made of SAE 1030 was quenched in water. Under these circumstances, the maximum temperature difference appears during the transformation of the core but before martensite transformation of the surface starts. From the systematization of Wyss, it must be concluded that the wire-reel shape should result. However, the experiment has shown a spherical size distortion. The reason for this can be found in the stress development. When the maximum temperature difference occurs, the core is under compressive stress (Fig. 15). If the transformation starts here, the increase of specific volume leads to an additional compressive stress. Therefore, the stress situation equates an amplified thermal stress condition with the known result in size and shape changes.

Maximum Temperature Difference and Concurrent Transformations over the Complete Cross Section. In the last example (Fig. 22d), a water-quenched cylinder made from AISI 3310 with a diameter of 100 mm (4 in.) was tested. In this case, point W occurs simultaneously with the martensitic transformation of the surface, before the core starts to form pearlite. Therefore, the wire-reel distortion results.

The Influence of Biot and Other Dimensionless Numbers on Size Changes. In the preceding paragraphs, simple two-shell models were used to explain qualitatively the resulting distortion. This worked quite well for the examples in Fig. 22(a) through (c). However, for the example in Fig. 22(d), the result cannot be concluded by such a simple argument. Furthermore, heat treatment simulations of transformation-free quenching processes have shown that Wyss's systematization is correct only for larger Biot numbers (Fig. 18). Therefore, it must be concluded that simple arguments can explain many but not all results. The reason is simply the complexity of distortion and stress generation.

Martensitic Hardening. Even in the simple case of pure martensitic hardening of a ring with a conical cross section, 30 parameters govern the distortion generation during quenching, and 26 dimensionless numbers are necessary to describe the problem (Ref 21). In addition to the well-known Biot and Fourier numbers, for example, the martensite-start (M_s) number:

$$\frac{M_s - T_\infty}{T_0 - T_\infty}$$

that compares the temperature difference between the martensite-start and coolant temperature with the maximum possible temperature difference (hardening temperature minus coolant) is an important number and has a huge influence on dimensional changes. Another important number is the so-called Koistinen-Marburger number:

$$\frac{T_0 - T_\infty}{M_0}$$

where M_0 is a material parameter that describes the kinetic of martensite formation. The dimensional alterations also are sensitive to changes of this parameter.

The thermal strain number:

$$\frac{(1+\nu)\cdot\alpha\cdot(T_0 - T_\infty)}{1 - 2\cdot\nu}$$

governs one of the dilatational terms in the thermoelastic part of the constitutive equations and is defined by Poisson's ratio (ν) and the thermal expansion coefficient (α). The sensitivity of dimensional alterations for variations in this number is similar to the numbers mentioned previously.

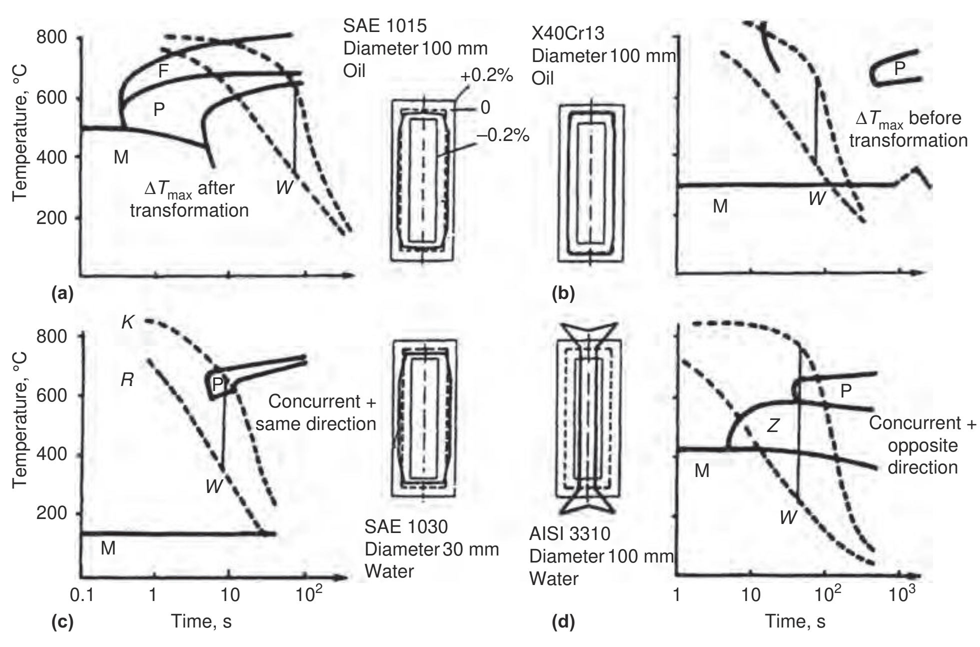

Fig. 22 Size and shape changes after hardening due to different interactions between thermal and transformation stresses. Courtesy of T. Lübben. Source: Ref 23

The second dilatational term, the transformation strain number:

$$\frac{(1+\nu)\cdot(\rho_a-\rho_m)}{3\cdot(1-2\cdot\nu)\cdot\rho_m}$$

compares the density difference of austenite and martensite. The influence on dimensional changes is smaller than the effects of the other numbers, but not negligible.

Definitions of the other dimensional numbers governing a through-hardening process are given in Ref 21. They characterize the elastic and plastic behavior of the material and define the ratio of properties of the martensite and austenite phases.

Hardening and Case-Hardening Processes with Diffusion-Controlled Phase Transformations. If diffusion-controlled transformations must be taken into account and/or a case-hardening process should be judged, the number of parameters increases dramatically. Additionally, it should not be forgotten that the hypothetical experiment assumes many hypotheses that are not true in the real world of a heat treater. In such situations, only a heat treatment simulation can provide ideas about the interactions of the various mechanisms. (See the article, "Modeling and Simulation of Steel Heat Treatment: Prediction of Microstructure, Distortion, Residual Stress and Cracking" in this Volume.)

The Influence of Biot Number on Residual Stresses after a Through-Hardening Process. The examples in Fig. 21(a) and (b) demonstrate that for a fully martensitic hardening, the sign of the residual stresses depends on the cooling rate and the Biot number. To improve the fatigue limit of components, the generation of compressive residual stresses at the surface is necessary. Therefore, Rath investigated the influence of the Biot number on stress development for through hardening of cylinders made of the bearing steel SAE 52100 (Ref 24). Figure 23(a) shows the temporal development of axial surface stresses for different Biot numbers (defined according to Eq 13). All curves are qualitatively similar. The largest quantitative difference occurs between the start of the transformation at the surface (at approximately the maximum tensile stress) and at the core (minimum of the curves).

Figure 23(b) shows the residual-stress distribution in the radial direction. For a smaller Biot number, a continuous increase from compressive stresses in the core to tensile stresses at the surface was found. For higher Biot number values, a stress maximum near the surface is formed. Further increase of the Biot number moves this maximum to deeper regions of the cylinder, and the surface stresses become negative. Consequently, there must be a critical Biot number for zero stresses at the surface (here: between 2 and 8).

Figure 24 shows the residual stresses at the surface as a function of the Biot number for different combinations of surface and volume. First, it can be seen that the concept of a Biot number also works here. The curve is practically independent from the values of characteristic length and heat-transfer coefficient. Only the value of the Biot number is important. Secondly, Fig. 24 shows that a critical Biot number exists (here: approximately 2.75). To produce compressive residual stresses at the surface of the cylinder under the given conditions, a minimal value of 2.75 is necessary.

Up until now, the final microstructure of all presented results in this section consisted of martensite and 12% retained austenite. However, what happens when the austenitizing conditions and therefore the martensite-start temperature and the martensite-formation rate are changed? To answer this question, Rath performed systematical variations of these two parameters by using the Koistinen-Marburger law to calculate martensite formation. (For details, see the article "Modeling and Simulation of Quenching, Residual Stress, Distortion, and Quench Cracking Formation" in this Volume.) Figure 24(b) shows that for larger values of M_s, comparably small critical Biot numbers (Bi_{crit}) result that are practically independent from the Koistinen-Marburger parameter (k). With decreasing martensite-start temperatures, Bi_{crit} increases, and a strong influence of k occurs.

Other material properties also influence the development of stresses. According to the investigations of Rath, the thermal expansion coefficient has the largest influence on the critical Biot number (Ref 25). Furthermore, the elastic properties of both phases and the thermal expansion coefficient of martensite also have significant influence.

Quenching processes resulting in larger Biot numbers are called intensive quenching. Many investigations concerning this topic were done by Kobasko and Aronov and are presented in the Division "Quenchants and Quenching Technologies" in this Volume.

Avoidable Size and Shape Changes

In practice, it is impossible to approach the ideal conditions mentioned in the hypothetical experiment in the previous section. However, what are the important points if the real conditions must be taken into account?

Distortion Potential

Figure 25 shows some examples of real conditions. In general, heat treatment of crown wheels leads to enormous distortion (Fig. 25a). Therefore, such parts normally are hardened in quenching presses. What is the main reason for this result? It easily can be seen that in the regions of the tooth, the surface is larger and the volume is smaller compared to the lower part of the wheel. Consequently, the tooth cools down much faster, and thermal stresses rise between the upper and lower parts.

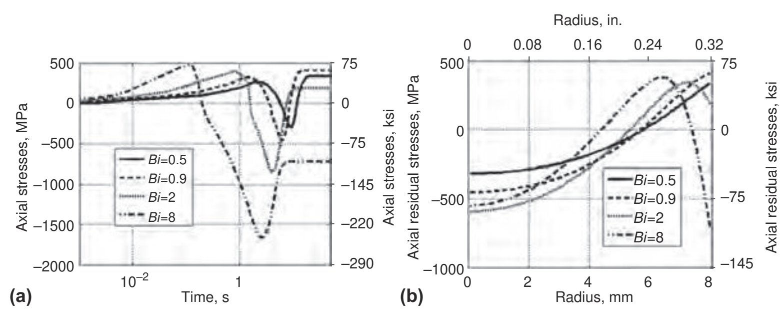

Fig. 23 (a) Influence of Biot number (Bi) on the development of axial stresses at the surface of cylinders. (b) Radial distribution of corresponding residual axial stresses in the middle plane of cylinders. Courtesy of Wolfson Heat Treatment Centre, IFHTSE, and Maney Publishing. Source: Ref 24

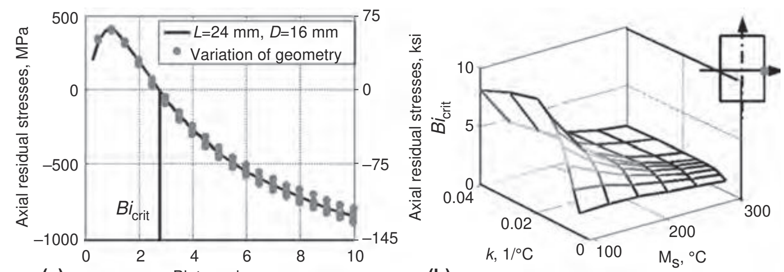

Fig. 24 (a) Simulated residual stresses at the surface of cylinders (100Cr6, SAE 52100) as a function of the Biot number. (b) Critical Biot number (Bi_{crit}) for compressive stresses at the surface showing dependence of martensite-start temperature (M_s) and Koistinen-Marburger parameter (k). Courtesy of Wolfson Heat Treatment Centre, IFHTSE, and Maney Publishing. Source: Ref 24

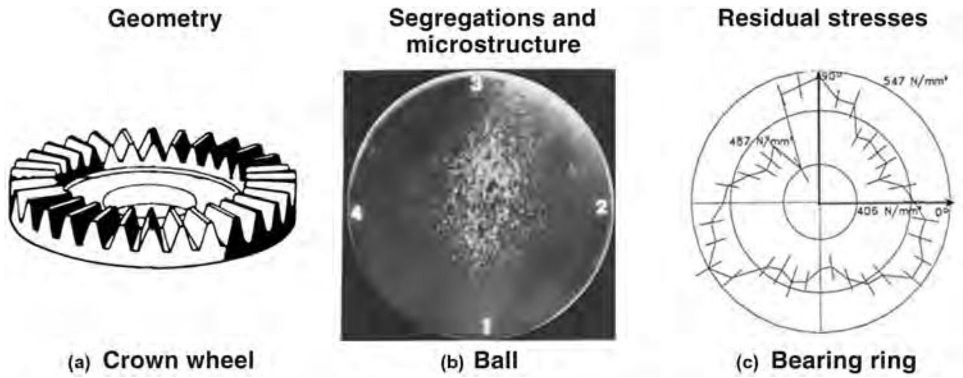

Fig. 25 Real conditions and distortion potential. Courtesy of Wolfson Heat Treatment Centre, IFHTSE, and Maney Publishing. Source: Ref 26

This can cause a tilting of the complete gear, even if all other influencing parameters are as perfect as assumed in the theoretical experiment. The reason for this shape change is the asymmetry of mass distribution of the crown wheel—its geometry.

In the Fig. 25(b), the ball is no longer spherical but ellipsoid after hardening. After cutting it in the direction of the longest axis of the ellipsoid, an inhomogeneous, asymmetric distribution of microstructure was found. This asymmetry results from an asymmetric distribution of the chemical composition, known as segregation. These two distributions cause complex interactions during heat treatment. The differences in the microstructure result in local differences of volume change during austenitizing, and therefore, transformation stresses occur. Furthermore, variations in the chemical composition provoke an asymmetric, position-dependent transformation behavior and therefore complex distributions of stress and strain development.

After heat treatment, the ring in Fig. 25(c) exhibits a large third-order amplitude in the Fourier spectrum of its roundness plot. The distribution of residual stresses measured by x-ray after machining shows a triangularity similar to the roundness plot after heat treatment. It results from the interaction of clamping and turning during the machining process. During heating, these stresses are reduced by plastic deformations that give the resulting size and shape changes. More details are provided in Ref 27.

Following these examples, it can be concluded that not only the visible asymmetry or inhomogeneity of the mass distribution causes distortion, but also the invisible asymmetries of other properties can create distortion by complicated interactions during heat treatment. If a component inhibits such asymmetries, it contains a potential for distortion that will be set free during heat treatment and cause measureable size and shape changes. This potential is called the distortion potential of a component and cannot be measured. Measurable quantities are the carriers of the distortion potential.

Carriers of Distortion Potential

The carriers of distortion potential are the distributions of:

- Mass (geometry)
- All relevant alloying elements
- Microstructure, including grain size
- Stresses and residual stresses
- Mechanical history
- Temperature

From the viewpoint of process chain simulation, these carriers, with the exception of geometry, are the distributions of the state variables at the end of a process within the manufacturing chain and must be given as initial conditions for the simulation of the next process. However, to understand distortion generation, the interactions of the state variables during the processes must be analyzed. This can be done by process chain simulations (Ref 28– 30).

In the following sections, the carriers of distortion potential are discussed.

Mass Distribution. Geometry/mass distribution plays a particular role. On the one hand, asymmetries in mass distribution can result in distortion even under perfect conditions, as discussed for the crown wheel in the section "Distortion Potential" in this article. For this reason, a considerable amount of distortion potential is often created during the design phase of a component. According to Ref 31, this amount already reaches approximately 60% of the total potential of case-hardened gears.

On the other hand, distributions of the state variables are defined only in the corresponding volume and the process parameters, such as working stresses as well as heat and mass fluxes (e.g., carbon flux), acting over the surface of this volume. Furthermore, geometry plays an active role in distortion generation because the stress and strain distributions depend on it. In particular, the stress component normal to the surface must be zero. Therefore, a given geometry has something similar to a transfer function. This function defines the reaction of the geometry to deviations in the carriers from homogeneity. For bearing races with a rectangular cross section, development of the corresponding transfer function is given in Ref 27 and 32.

Distributions of All Relevant Alloying Elements and Microstructure, Including Grain Size. The distributions of the alloying elements and the distributions of microstructure and grain size are closely linked. Depending on the local curve, regions with higher amounts of alloying elements can form more martensite. Therefore, in many cases a banded microstructure can be used as an indicator for corresponding variations of alloying elements. Nevertheless, if the cooling rate everywhere is larger than the highest critical cooling rate, then no banded microstructure will result. This is the reason why, in general, the alloying elements and microstructure of the carriers must be analyzed individually.

These distributions cause complex interactions during heat treatment. The differences in the initial microstructure result in local differences of volume change during austenitizing, and therefore, transformation stresses occur. Furthermore, variations in the chemical composition provoke position-dependent transformation behavior and therefore complex distributions of stress and strain development. If these distributions have the same symmetries as the mass distribution of the components, only the size changes will be influenced. However, if asymmetries occur, then additional shape changes can result.

A detailed analysis of this topic is presented in the article "Distortion Engineering" in this Volume.

Distribution of Stresses and Residual Stresses. The role of symmetric stress distributions during a heat treatment process was discussed in the section "Systematization of Unavoidable Size and Shape Changes and Corresponding Stress Evolution" in this article. If one of the following occurs, then the plastic deformations also will become asymmetric:

- Asymmetries in other carriers, which have consequences for the degree of symmetry of stress distribution
- Nonsymmetrical distribution of residual stresses after forming or machining processes
- Dead load acts in an asymmetrical way on the component.

Consequently, additional shape changes will occur.

Dead Load and Friction. Figure 26 shows roundness plots of thin-walled rings (145 mm diameter by 133 mm diameter by 26 mm, or 6 by 5 by 1 in.) made of SAE 52100. These plots are oriented parallel to the linear supports used during heat treatment. This behavior results from friction between the rings and the support tools, which generates small stresses in the rings during the heating process. The plastic deformations result from creep and transformation plasticity during the formation of austenite. These mechanisms were identified by heat treatment simulations that took into account the contact between ring and support (Ref 27, 33).

Residual Stresses. Another important factor is the distribution of residual stresses resulting from processes before heat treatment. Figure 27 shows the results of tests with cold formed rings. After the forming process, these rings have residual stresses of −100 to −200 MPa (−15 to −30 ksi) over the complete cross section (Ref 34). After an annealing process with a temperature between 300 and 700 °C (570 and 1290 °F), roundness plots and residual stress were measured. Figure 27(a) shows that with increasing annealing temperature, radius and ovality changes increase. Figure 27(b) indicates the reason for this result: The average residual stresses were reduced over the complete cross section. Therefore, elastic strains occur, and thus, a radius change results. The ovality increase must be explained by an inhomogeneity in the residual-stress distribution after cold forming that becomes smaller during the heating process. The measurements presented in Ref 34 show this effect principally, but as discussed in Ref 27, many more measurements or simulations are necessary to demonstrate this mechanism unambiguously. Furthermore, strain hardening during cold forming is increased. Therefore, the mechanical history, as discussed in the next section, also should play an important role. However, these two effects can be separated only by a coupled simulation of forming and heat treatment.

Distribution of Mechanical History. The role of mechanical history consists of the influence of plastic deformations on effects occurring after the plasticization. One effect is the strain-hardening behavior (Bauschinger effect). Kinematic or isotropic behavior or mixtures thereof are discussed in this section; more details can be found elsewhere (Ref 35).

During forming processes, very high degrees of deformation occur. In this case, recrystallization effects must be taken into account. Finally, the mechanical history can have an influence on the transformation behavior.

Temperature Distribution. The very important role of temperature already was highlighted during the discussion of unavoidable size and shape changes. The avoidable distortions, inhomogeneities, and asymmetries in the temperature distribution resulting not from mass distribution but from heat-transfer conditions and therefore from the process must be taken into account. The imperfections in the temperature distribution resulting from these nonperfect conditions must be added to the effects coming from the geometry itself and causing mainly additional shape changes.

Distortion—A System Property

Figure 28 shows schematically a typical process chain for bearing race manufacturing and some possible modifications of the carriers along the process chain. The geometry and the appropriate distortion potential were defined previously in the design step. During casting, the chemical composition of the melt and the corresponding segregations result, and another part of the distortion potential was inserted into the component. Geometric modification during the forming processes also changes the distributions of segregations. Furthermore, the first changes of the mechanical history occur. During soft machining, residual stresses will be generated, and the corresponding plastic deformations modify the mechanical history. Additionally, there will be an interaction between these two carriers of distortion potential. Similar effects happen during heating. The quenching step releases the distortion potential of the segregations and microstructure by phase transformations, with strong interactions between both carriers.

The message of these examples is that modifications of the carriers of distortion potential can happen during the complete processing

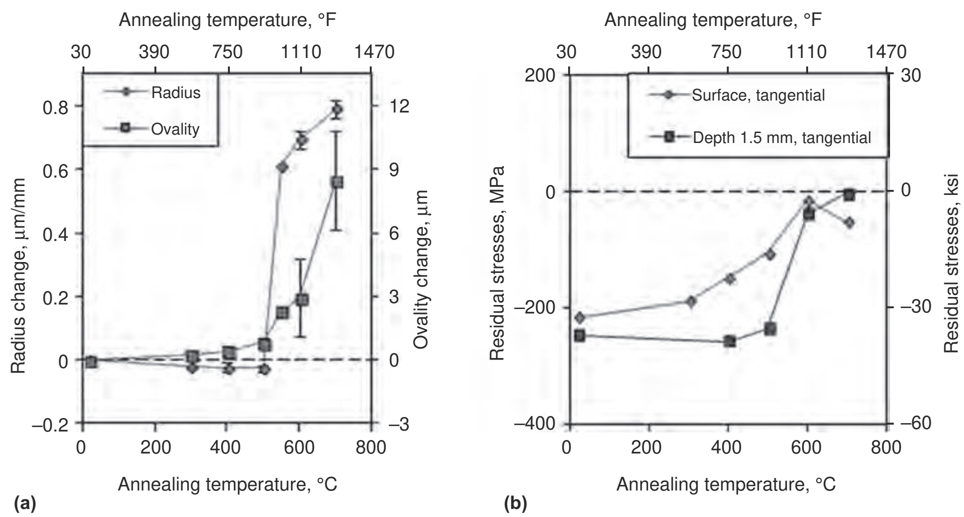

Fig. 27 (a) Radius and ovality changes and (b) corresponding residual stresses during heating of cold rolled rings. Courtesy of H. Surm. Source: Ref 33

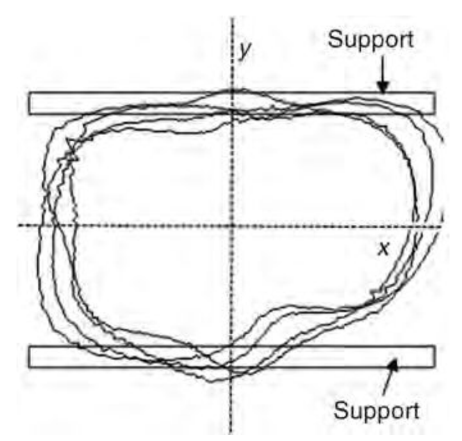

Fig. 26 Characteristic roundness plots after heat treatment of thin-walled bearing races by use of linear loading tools. Courtesy of H. Surm. Source: Ref 33

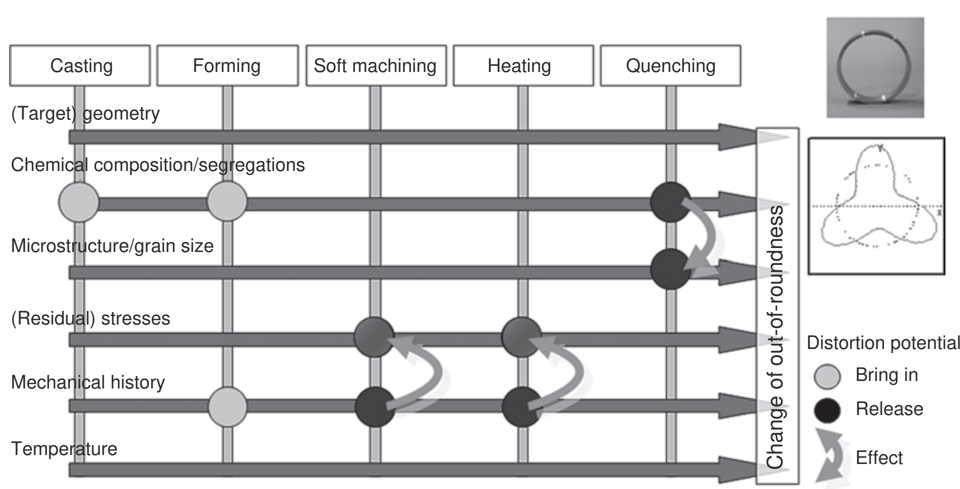

Fig. 28 Possible changes and interactions of distortion potential carriers along the process chain. Source: Ref 36

of a component from the design phase through casting, rolling or forming, soft machining, heat treatment, and hard machining. Therefore, distortion is not a problem of heat treatment alone. Distortion is a system property, and distortion control during manufacturing processes must follow a system-oriented approach. The corresponding system is the complete manufacturing chain. According to studies carried out for bearing races in particular, there are more than 200 parameters that may be relevant (Ref 37). This is likely the reason that a system-oriented view of component distortion, emphasizing the relationships between the individual production steps, can be found only sporadically in the industry today (2014) (Ref 26).

The Role of Heating, Austenitizing, and Carburizing

In general, studies about the influence of heat treatment on distortion focus on the quenching process. However, it must be noted that heating, austenitizing, and carburizing also can be responsible, to a great degree, for the generation of distortion. During these processes, the thermal stresses are small in many cases. Therefore, in general, yielding plasticity does not play a major role, but transformation plasticity and creep can have a nonnegligible effect (Ref 27). Furthermore, anisotropic effects, which result from segregations, must be taken into account, especially during heating (Ref 30, 38).

ACKNOWLEDGMENTS

Since 1990, an expert panel of the German heat treatment association AWT worked continuously on a distortion monograph (Ref 5, written in German). In 2012, the fourth edition of this book appeared, and a total of 32 authors from industry and universities wrote parts of it. The author would like to thank the members of this expert panel for their approval to translate some sections of this monograph and publish it in this *ASM Handbook*.

In the period from 2001 to 2011, the Collaborative Research Center (CRC) "Distortion Engineering—Distortion Control during Manufacturing Processes" was financed by the Deutsche Forschungsgemeinschaft (DFG) (German Research Foundation). During this time, much knowledge was developed concerning the basics of distortion generation, which was used in this article. The author would like to thank the DFG for the funding and all members of the CRC for their generous cooperation and many fruitful discussions.

REFERENCES

1. S. Gunnarson, Einfluss der Stranggussform auf den Verzug eines einsatzgehärteten Tellerrades aus Stahl, *Härt.-Tech. Mitt.*, Vol 46 (No. 4), 1991, p 216–220
2. J. Volkmuth, S. Lane, M. Jung, and U. Sjöblom, Einfluss ungleichmäßiger Eigenspannungen in Wälzlagerringen vor dem Härten auf Formabweichungen nach dem Härten, *HTM Z. Werkstofftech. Wärmebeh. Fertigung*, Vol 60 (No. 6), 2005, p 317–322
3. I.N. Bronstein and K.A. Semendjajew, *Taschenbuch der Mathematik*, Vol 20, Verlag Harri Deutsch, Thun und Frankfurt/Main, 1981
4. T. Lübben and H.-W. Zoch, Einführung in die Grundlagen des Distortion Engineering, *HTM J. Heat Treat. Mater.*, Vol 67 (No. 5), 2012, p 275–290
5. K. Heeß and 31 coauthors, *Maß- und Formänderungen infolge Wärmebehandlung von Stählen*, 4th ed., Expert Verlag, Renningen, 2012 (in German)
6. U. Ahrens, G. Besserdich, and H.J. Maier, Effect of Stress on the Bainitic and Martensitic Phase Transformation Behavior of a Low Alloy Tool Steel, *Advances in Mechanical Behavior, Plasticity and Damage*, Vol 2, D. Miannay, P. Costa, D. Francois, and A. Pineau, Ed., Euromat 2000, Elsevier, Oxford, 2000, p 817–822
7. B.S. Lement, *Distortion in Tool Steels*, American Society for Metals, Metals Park, OH, 1959
8. G. Besserdich, "Untersuchungen zur Eigenspannungs- und Verzugsausbildung beim Abschrecken von Zylindern aus den Stählen 42CrMo4 und Ck45 unter Berücksichtigung der Umwandlungsplastizität," Dissertation, Universität Karlsruhe (TH), 1993
9. M. Dalgic and G. Löwisch, Transformation Plasticity at Different Phase Transformation of Bearing Steel, *Mater.wiss. Werkst. tech.*, Vol 37 (No. 1), 2006, p 122–127
10. G. Besserdich, H. Müller, and E. Macherauch, Experimentelle Erfassung der Umwandlungsplastizität und ihre Auswirkungen auf Eigenspannungen und Verzüge, *Härt.-Tech. Mitt.*, Vol 50 (No. 6), 1995, p 389–396
11. M. Hunkel, Anisotropic Transformation Strain and Transformation Plasticity: Two Corresponding Effects, *Mater.wiss. Werkst. tech.*, Vol 40 (No. 5–6), 2009, p 466–472
12. U. Wyss, Die wichtigsten Gesetzmäßigkeiten des Verzuges bei der Wärmebehandlung des Stahles, *Wärmebehandlung der Bau- und Werkzeugstähle*, H. Benninghoff, Ed., BAZ Buchverlag Basel, 1978
13. A. Rose, Eigenspannungen als Ergebnis von Wärmebehandlung und Umwandlungsverhalten, *Härt.-Tech. Mitt.*, Vol 21 (No. 1), 1966, p 1–6
14. E. Ameen, Dimension Changes of Tool Steels during Quenching and Tempering, *Trans. ASM*, Vol 28, 1940, p 472–512
15. R. Chatterjee-Fischer, Beispiele für durch Wärmebehandlung bedingte Eigenspannungen und ihre Auswirkungen, *Härt.-Tech. Mitt.*, Vol 28, 1973, p 276–288
16. F. Frerichs, D. Landek, T. Lübben, F. Hoffmann, and H.-W. Zoch, Prediction of Distortion of Cylinders without Phase Transformations, *First Int. Conf. on Distortion Engineering (IDE)*, (Bremen, Germany), 2005, p 415–423
17. F. Frerichs, T. Lübben, F. Hoffmann, H.-W. Zoch, and M. Wolff, Unavoidable Distortion due to Thermal Stresses, *Fifth Int. and European Conference on Quenching and Control of Distortion*, (Berlin, Germany), 2007, p 145–156
18. N.I. Kobasko, V.S. Morganyuk, and V.V. Dobrivecher, Control of Residual Stress Formation and Steel Deformation during Rapid Heating and Cooling, *Handbook of Residual Stress and Deformation of Steel*, G. Totten, M. Howes, and T. Inoue, Ed., ASM International, Materials Park, OH, 2002, p 312–330
19. C. Hutter and K. Jöhnk, *Continuum Methods of Physical Modelling—Continuum Mechanics, Dimensional Analysis, Turbulence*, Springer, Berlin, Heidelberg, 2004
20. D. Landek, D. Lisjak, F. Frerichs, T. Lübben, F. Hoffmann, and H.-W. Zoch, Prediction of Unavoidable Distortions in Transformation-Free Cooling by a Newly Developed Dimensionless Model, *Second Int. Conf. on Distortion Engineering (IDE)*, (Bremen, Germany), 2008, p 237–246
21. C. Şimşir, T. Lübben, F. Hoffmann, and H.-W. Zoch, Dimensional Analysis of the Thermomechanical Problem Arising during Through-Hardening of Cylindrical Steel Components, *Comput. Mater. Sci.*, Vol 49, 2010, p 462–472
22. R. Schröder, B. Scholtes, and E. Macherauch, Rechnerische und röntgenographische Analyse der Eigenspannungsbildung in abgeschreckten Stahlzylindern, *Härt.-Tech. Mitt.*, Vol 39, 1984, p 280–291
23. T. Lübben and H.W. Zoch, Introduction to the Basics of Distortion Engineering, *HTM J. Heat Treat. Mater.*, Vol 5, 2012, p 275–290
24. J. Rath, T. Lübben, F. Hoffmann, and H.-W. Zoch, Generation of Compressive Residual Stresses by High-Speed Water Quenching, *Int. Heat Treat. Surf. Eng.*, Vol 4 (No. 4), 2010, p 156–159, www.maneyonline.com/iht
25. J. Rath, "Maximierung der randnahen Druckeigenspannung von Stählen mit Hilfe einer Hochgeschwindigkeits—Abschreckanlage," Dissertation, Universität Bremen, 2013
26. F. Hoffmann, O. Kessler, T. Lübben, and P. Mayr, Distortion Engineering—Distortion Control during the Production Process, *Heat Treat. Met.*, Vol 2, 2004, p 27–30, www.maneyonline.com/iht
27. T. Lübben, F. Hoffmann, and H.-W. Zoch, Distortion Engineering: Basics and Application to Practical Examples of Bearing Races, in *Comprehensive Materials Processing*, G. Krauss, *Thermal Engineering of Steel and Other Alloy Systems*, Elsevier, 2013

28. V. Schulze, R. Pabst, and H. Meier, Research Training Group 1483, Process Chains in Manufacturing: Interaction, Modelling and Evaluation of Process Zones, *Proc. Third Int. Conf. on Distortion Engineering (IDE)*, (Bremen, Germany), 2011, p 421–428
29. U. Prahl, G.J. Schmitz, S. Benke, S. Konovalov, S. Freyberger, T. Henke, and M. Bambach, Integrative Computational Materials Engineering towards Distortion Prediction, *Proc. Third Int. Conf. on Distortion Engineering (IDE)*, (Bremen, Germany), 2011, p 429–436
30. C. Şimşir, M. Hunkel, J. Lütjens, and R. Rentsch, Process-Chain Simulation for Prediction of the Distortion of Case-Hardened Gear Blanks, *Mater.wiss. Werkst.tech.*, Vol 43 (No. 1–2), 2012, p 163–170
31. C.M. Bergström, L.-E. Larsson, and T. Lewin, Reduzierung des Verzuges beim Einsatzhärten, *Härt.-Tech. Mitt.*, Vol 43, 1988, p 36–40
32. F. Frerichs, T. Lübben, F. Hoffmann, and H.-W. Zoch, Ring Geometry as an Important Part of Distortion Potential, *Mater. wiss. Werkst.tech.*, Vol 43 (No. 1–2), 2012, p 16–22
33. H. Surm and J. Rath, Mechanismen der Verzugsentstehung bei Wälzlagerringen aus 100Cr6, *HTM J. Heat Treat. Mater.*, Vol 67 (No. 5), 2012, p 291–303
34. J. Epp, H. Surm, T. Hirsch, and F. Hoffmann, Residual Stress Relaxation during Heating of Bearing Rings Produced in Two Different Manufacturing Chains, *J. Mater. Process. Technol.*, Vol 211, 2011, p 637–643
35. C. Şimşir, M. Dalgic, T. Lübben, A. Irretier, M. Wolff, and H.-W. Zoch, The Bauschinger Effect in the Supercooled Austenite of SAE 52100 Steel, *Acta Mater.*, Vol 58, 2010, p 4478–4491
36. H.-W. Zoch and T. Lübben, Verzugsarme Wärmebehandlung niedrig legierter Werkzeugstähle, *HTM J. Heat Treat. Mater.*, Vol 65 (No. 4), 2010, p 209–218
37. J. Volkmuth, Eigenspannungen und Verzug, *Härt.-Tech. Mitt.*, Vol 51 (No. 3), 1996, p 145–154
38. M. Hunkel, Modelling of Phase Transformations and Transformation Plasticity of a Continuous Casted Steel 20MnCr5 Incorporating Segregations, *Mater.wiss. Werkst.tech.*, Vol 43 (No. 1–2), 2012, p 150–157

SELECTED REFERENCES

- H. Berns, Verzug von Stählen infolge von Wärmebehandlung, *Z. Werkstofftech.*, Vol 8, 1977, p 149–157
- F. Frerichs, D. Landek, T. Lübben, F. Hoffmann, and H.-W. Zoch, Prediction of Distortion of Cylinders without Phase Transformations, *Mater.wiss. Werkst.tech.*, Vol 37 (No. 1), 2006, p 63–68
- J. Pan, Factors Affecting Final Part Shaping, *Handbook of Residual Stress and Deformation of Steel*, G. Totten, M. Howes, and T. Inoue, Ed., ASM International, Materials Park, OH, 2002, p 159–182
- G.E. Totten, C.E. Bates, and N.A. Clinton, *Handbook of Quenchants and Quenching Technology*, ASM International, Materials Park, OH, 1993